Proceedings of ASME 2015 Dynamic Systems and Control Conference
DSCC 2015
October 28-30, 2015, Columbus, Ohio, USA

DSCC2015-9993

HIERARCHICAL DESIGN FOR CONNECTED CRUISE CONTROL

Linjun Zhang*
Department of Mechanical Engineering
University of Michigan
Ann Arbor, Michigan 48109
Email: linjunzh@umich.edu

Chaozhe He
Department of Mechanical Engineering
University of Michigan
Ann Arbor, Michigan 48109
Email: hchaozhe@umich.edu

Jing Sun
Department of Naval Architecture & Marine Engineering
University of Michigan
Ann Arbor, Michigan 48109
Email: jingsun@umich.edu

Gábor Orosz
Department of Mechanical Engineering
University of Michigan
Ann Arbor, Michigan 48109
Email: orosz@umich.edu

ABSTRACT

In this paper, we propose a hierarchical framework to reduce the design complexity of connected cruise control (CCC), which is used to regulate the longitudinal motion of a vehicle by utilizing wireless vehicle-to-vehicle (V2V) communication. A high-level controller is designed to generate desired motion of the CCC vehicle based on the motion of multiple vehicles ahead. A low-level controller is used to regulate the engine torque and select the appropriate gear to enable the vehicle to track the desired motion. To cope with external disturbances and uncertain physical parameters, we use an adaptive control strategy for the low-level controller. In a case study, we design a specific CCC algorithm by using the presented hierarchical framework. Numerical simulations are used to validate the analytical results and test the system performance.

1 INTRODUCTION

Exploiting wireless vehicle-to-vehicle (V2V) communication in vehicle control systems has a great potential to improve traffic efficiency, enhance vehicle safety, and reduce fuel consumption [1–3]. The main advantage of V2V communication is the ability to monitor the motion of vehicles that are beyond the line of sight. One way to utilize V2V communication is using cooperative adaptive cruise control (CACC) in a platoon of vehicles where each vehicle senses the motion of the vehicle immediately ahead by using range sensors (e.g., radar) and also monitors the motion of the designated leader via V2V communication [4, 5]. Although CACC platoon has been realized experimentally [6–9], deploying CACC in real traffic is difficult since it requires radar-equipped vehicles to travel next to each other, which rarely occurs in practice due to the low penetration of such vehicles. Moreover, CACC requires that all vehicles communicate with the designated leader, which strongly restricts the structure of the communication network and limits the length of the platoon by the communication range. To increase the length of CACC platoon, vehicles may relay the information received from the leader. However, this increases the effective delay and the complexity, and thus it is not used in practice.

To relax the aforementioned limitations, connected cruise control (CCC) was proposed in [10–12], which requires neither a designated leader nor a prescribed connectivity structure while also allowing the incorporation of human-driven vehicles. Due to the high flexibility, CCC can be implemented in traffic with low penetration of vehicles equipped with range sensors and/or V2V

*Address all correspondence to this author.

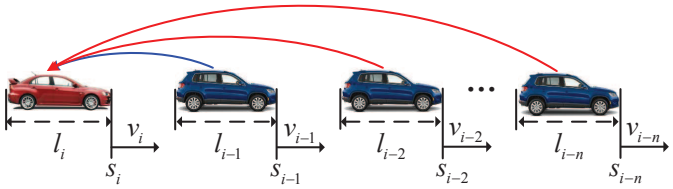

FIGURE 1. Vehicle network where a CCC vehicle (red) receives information from multiple vehicles ahead. Symbols s_j, l_j and v_j denote the position, length and velocity of vehicle j, respectively. The blue link can be realized by human perception, range sensors, and V2V communication while red links can only be realized by V2V communication.

communication devices. When designing CCC, typically the desired acceleration is designed by using simplified vehicle models where external disturbances (headwind, road grade, and rolling resistance, etc.) are neglected and vehicle parameters (mass, air drag coefficient, etc.) are assumed to be known. However, to implement the controller on a real vehicle, one must consider the physical relationship between the acceleration and the engine torque, which is influenced by external disturbances and parameter uncertainties. In this paper, we propose a hierarchical framework for CCC design. At the high level, a simplified vehicle model is used to design controllers to achieve certain goals such as string stability [13–15], optimal fuel consumption [16], and collision avoidance [17]. At the low level, an adaptive control strategy is designed to regulate the engine torque and switch gears so that the vehicle follows the desired motion despite external disturbances and parameter uncertainties.

The rest of this paper is organized as follow. In Section 2, we provide a hierarchical framework for CCC design and derive corresponding stability conditions. In Section 3, we present a case study to demonstrate the applicability of the proposed control strategy and use numerical simulations to evaluate the system performance. Conclusions and future research directions are provided in Section 4.

2 HIERARCHICAL DESIGN FRAMEWORK FOR CONNECTED CRUISE CONTROL

The objective for CCC design is to achieve certain system-level performance (e.g., string stability, minimal fuel consumption, etc.) by utilizing the motion data received via V2V communication. In this section, we propose a hierarchical framework to reduce the complexity of CCC design.

In Fig. 1, vehicle i (red) monitors the positions s_j and the velocities v_j of vehicles $j = i-1,\ldots,i-n$ within the effective communication range. The symbol l_j denotes the length of vehicle j. Note that the vehicle immediately ahead can be monitored by the human perception, by range sensors (e.g., radar), or by V2V communication while distant vehicles can only be monitored by V2V communication. We emphasize that CCC does not require all vehicles $i-1,\ldots,i-n$ to be equipped with range sensors and/or communication devices. In fact, all of these vehicles may be human-driven while a few of them broadcast information.

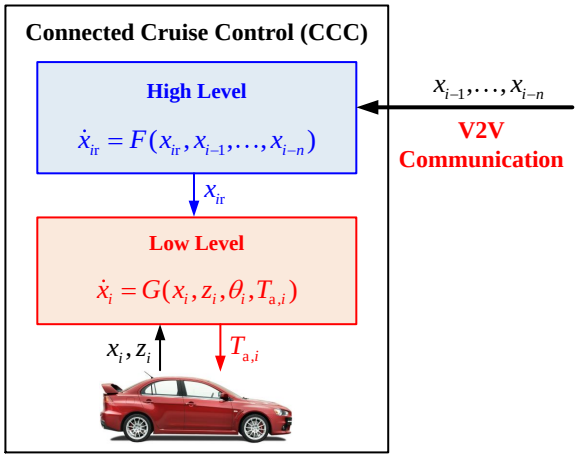

FIGURE 2. A hierarchical framework for CCC design that utilizes the motion data $x_j = [s_j, v_j]^{\mathrm{T}}$ from vehicles $j = i-1,\ldots,i-n$ received via V2V communication. The high-level controller determines the desired state $x_{ir} = [s_{ir}, v_{ir}]^{\mathrm{T}}$. At the low level, the axle torque $T_{a,i}$ is designed to enable the vehicle state $x_i = [s_i, v_i]^{\mathrm{T}}$ to track the desired state x_{ir} while taking into account the external disturbances z_i and the physical parameters θ_i.

A hierarchical framework for CCC design is presented in Fig. 2. At the high level, by using a simplified vehicle model, we utilize the motion data $x_j = [s_j, v_j]^{\mathrm{T}}$ received from vehicles $j = i-1,\ldots,i-n$ in the connected car-following dynamics $\dot{x}_{ir} = F(x_{ir}, x_{i-1}, \ldots, x_{i-n})$, in order to determine the desired state $x_{ir} = [s_{ir}, v_{ir}]^{\mathrm{T}}$ of vehicle i. At the low level, the physical vehicle model $\dot{x}_i = G(x_i, z_i, \theta_i, T_{a,i})$ is used to design the axle torque $T_{a,i}$ so that the vehicle state x_i tracks the desired state x_{ir}. Here, the disturbance vector z_i includes the road grade and the headwind speed, while the parameter vector θ_i contains vehicle mass, rolling resistance coefficient, and air drag coefficient. In practice, θ_i is uncertain as the values of physical parameters may be unknown or vary over time. To deal with parametric uncertainties, the low-level controller is designed by using adaptive control [18].

2.1 High Level: Connected Car-Following Dynamics

At the high level, a simplified vehicle model is used to design the desired car-following dynamics of the CCC vehicle by using the motion data of multiple vehicles ahead, aiming to achieve certain system-level properties such as string stability and/or minimal fuel consumption. These properties require the asymptotic stability of the CCC vehicle, that is, if vehicles $j = i-1,\ldots,i-n$ move with identical constant speed v^*

such that

$$x_j^* = \begin{bmatrix} s_j^* \\ v_j^* \end{bmatrix} = \begin{bmatrix} v^* t + s_j^0 \\ v^* \end{bmatrix}, \tag{1}$$

for $j = i-n, \ldots, i-1$, where s_j^0 is a constant shift, then the CCC vehicle i shall approach the equilibrium

$$x_{i\mathrm{r}}^* = \begin{bmatrix} s_{i\mathrm{r}}^* \\ v_{i\mathrm{r}}^* \end{bmatrix} = \begin{bmatrix} v^* t + s_{i\mathrm{r}}^0 \\ v^* \end{bmatrix}. \tag{2}$$

Here, we use the word "headway" to describe the bumper-to-bumper distance between two consecutive vehicles, and define the average headway between vehicle j and vehicle i as

$$h_{i,j} = \frac{s_j - s_i - \sum_{k=j}^{i-1} l_k}{i-j}, \quad i > j. \tag{3}$$

We consider the connected car-following dynamics in the form

$$\begin{aligned} \dot{x}_{i\mathrm{r}} &= F(x_{i\mathrm{r}}, x_{i-1}, \ldots, x_{i-n}) \\ &= \begin{bmatrix} v_{i\mathrm{r}} \\ \sum_{j=i-n}^{i-1} \gamma_{i,j} \big(f_j(h_{i\mathrm{r},j}) + d_j(v_j) + g_j(v_{i\mathrm{r}}) \big) \end{bmatrix}, \end{aligned} \tag{4}$$

where $h_{i\mathrm{r},j}$ is given by (3) when replacing s_i with $s_{i\mathrm{r}}$. The continuously differentiable functions $f_j(h_{i\mathrm{r},j})$, $d_j(v_j)$, and $g_j(v_{i\mathrm{r}})$ determine the reaction to the average headway and relative velocity between vehicles i and j. The constants $\gamma_{i,j}$ describe the connectivity structure such that

$$\gamma_{i,j} = \begin{cases} 1, & \text{if vehicle } i \text{ utilizes data of vehicle } j, \\ 0, & \text{otherwise}. \end{cases} \tag{5}$$

In the remainder of this paper, we use $L \succ 0$ ($L \prec 0$) to denote positive (negative) definiteness of L. Note that L can be either a scalar or a matrix. Then, a sufficient condition for the asymptotic stability of the equilibrium (2) is stated as follow.

Theorem 1. *Suppose that the states of the vehicle network are bounded such that $h_{i\mathrm{r},j} \in \mathscr{D}_h$ ($j = i-n, \ldots, i-1$) and $v_{i\mathrm{r}} \in \mathscr{D}_v$. Then, the equilibrium* (2) *of the system* (4) *is asymptotically stable if there exists a Lyapunov function $L(x_{i\mathrm{r}}) \succ 0$ such that*

$$\left[\frac{\partial L(x_{i\mathrm{r}})}{\partial x_{i\mathrm{r}}} \right]^{\mathrm{T}} \frac{\partial F(x_{i\mathrm{r}}, x_{i-1}^*, \ldots, x_{i-n}^*)}{\partial x_{i\mathrm{r}}} x_{i\mathrm{r}} \prec 0 \tag{6}$$

holds for all $h_{i\mathrm{r},j} \in \mathscr{D}_h$ and $v_{i\mathrm{r}} \in \mathscr{D}_v$, where x_j^* is given by (1) *for $j = i-n, \ldots, i-1$.*

The proof of Theorem 1 is given in Appendix A. We remark that the region of attraction may be smaller than $\mathscr{D}_h \times \mathscr{D}_v$. Based on the asymptotic stability of the equilibrium, one can further investigate other properties such as string stability, minimal fuel consumption, and collision avoidance. But these are outside the scope of this paper.

2.2 Low Level: Adaptive Torque Control

The low-level controller acts on the axle torque $T_{\mathrm{a},i} = \eta_i T_{\mathrm{e},i}$, which is determined by the ratio η_i and the engine torque $T_{\mathrm{e},i}$. Note that η_i = gear ratio $\times$ final drive ratio; see Appendix D for parameters used for a heavy-duty vehicle. The control objective at the low level is to regulate $T_{\mathrm{a},i}$ such that the vehicle tracks the desired motion generated by the high-level controller, i.e.,

$$x_i(t) \to x_{i\mathrm{r}}(t), \quad \text{as } t \to \infty. \tag{7}$$

When designing the low-level controller, we use the physics-based model presented in [19, 20] where the flexibility of the suspension and the tire is neglected. That is,

$$\begin{aligned} \dot{x}_i &= G(x_i, z_i, \theta_i, T_{\mathrm{a},i}) \\ &= \begin{bmatrix} v_i \\ -\frac{mg}{m_{\mathrm{eff}}} \sin\phi_i - \frac{rmg}{m_{\mathrm{eff}}} \cos\phi_i - \frac{k}{m_{\mathrm{eff}}} (v_i + v_{\mathrm{w},i})^2 + \frac{1}{m_{\mathrm{eff}} R} T_{\mathrm{a},i} \end{bmatrix}, \end{aligned} \tag{8}$$

where the effective mass $m_{\mathrm{eff}} = m + J/R^2$ contains the vehicle mass m, the moment of inertia J of the rotating elements, and the wheel radius R. Moreover, g is the gravitational constant, r is the rolling resistance coefficient, k is the air drag coefficient. Finally, ϕ_i denotes the inclination angle of the road while $v_{\mathrm{w},i}$ is the speed of the headwind.

Multiplying the second equation in (8) by $m_{\mathrm{eff}} R$ yields

$$\theta_{i,1} \dot{v}_i = -\theta_{i,2} \sin\phi_i - \theta_{i,3} \cos\phi_i - \theta_{i,4} (v_i + v_{\mathrm{w},i})^2 + T_{\mathrm{a},i}, \tag{9}$$

where

$$\theta_{i,1} = m_{\mathrm{eff}} R, \quad \theta_{i,2} = mgR, \quad \theta_{i,3} = rmgR, \quad \theta_{i,4} = kR. \tag{10}$$

For compactness, we define the coefficient vector $\theta_i = [\theta_{i,1},\ \theta_{i,2},\ \theta_{i,3},\ \theta_{i,4}]^{\mathrm{T}}$.

We assume that the road grade ϕ_i and the headwind speed $v_{\mathrm{w},i}$ can be obtained by using on-board sensors, global positioning systems (GPS), and digital maps. Considering that the physical parameters may be uncertain in practice, we design an adaptive control strategy for the axle torque:

$$T_{\mathrm{a},i} = \hat{\theta}_i^{\mathrm{T}} w, \tag{11}$$

where $\hat{\theta}_i$ contains the parameters that shall adapt to the real values in θ_i and

$$w = \begin{bmatrix} \sum_{j=i-n}^{i-1} \gamma_{i,j}\big(f_j(h_{i,j}) + d_j(v_j) + g_j(v_i)\big) \\ \sin\phi_i \\ \cos\phi_i \\ (v_i + v_{\mathrm{w},i})^2 \end{bmatrix}. \tag{12}$$

Note that the first component of w is given by the high-level controller (4) by replacing s_{ir}, v_{ir} with s_i, v_i.

Defining the state tracking error as

$$e_i = x_{\mathrm{ir}} - x_i = \begin{bmatrix} e_{i,s} \\ e_{i,v} \end{bmatrix} = \begin{bmatrix} s_{\mathrm{ir}} - s_i \\ v_{\mathrm{ir}} - v_i \end{bmatrix}, \tag{13}$$

we present the adaptation law for the controller (11) as

$$\dot{\hat{\theta}}_i = \Gamma w \left[\frac{\partial L(e_i)}{\partial e_i}\right]_2, \tag{14}$$

where $\Gamma \in \mathbb{R}^{4\times 4}$ is a positive definite matrix consisting of the adaptation gains, w is given by (12), and $L(e_i)$ is the function used in Theorem 1 but replacing x_{ir} by e_i. Here, $[y]_k$ denotes the k-th element of the vector y. When implementing (14), we use a diagonal matrix $\Gamma = \mathrm{diag}\{\Gamma_1, \Gamma_2, \Gamma_3, \Gamma_4\}$, where $\Gamma_1, \ldots, \Gamma_4$ are positive scalars. Note that the adaptation speed of $\hat{\theta}_i$ depends on w given in (12). High adaptation speed may lead to undesired fast oscillations in transients. As the magnitude of w_4 is much larger than those of w_1, w_2, w_3 in (12), we choose the gain Γ_4 much smaller than Γ_1, Γ_2, Γ_3.

Applying the adaptive controller (11,14) to the system (8) with the reference model (4) yields an 8-dimensional closed-loop system with states $x_{\mathrm{ir}}, x_i \in \mathbb{R}^2$ and $\hat{\theta}_i \in \mathbb{R}^4$. This closed-loop system is excited by $2n$ inputs ($x_{i-1}, \ldots, x_{i-n}$ in (4)) and also contains 2 disturbances (ϕ_i and $v_{\mathrm{w},i}$ in (8)).

Theorem 2. *Suppose that Theorem 1 holds. The adaptive controller* (11) *with the adaptation law* (14) *can regulate the vehicle to track the desired motion in the sense of* (7)*.*

The proof is given in Appendix B. We remark that the controller (11) with the adaptation strategy (14) guarantees that x_i tracks x_{ir} but may not ensure the convergence of $\hat{\theta}_i$ to θ_i. This is discussed in Appendix B and will be demonstrated by using numerical simulations in Section 3.2.

3 CASE STUDY

In this section, we design a specific CCC strategy by applying the framework presented in Section 2. The derived controller is then applied to a heavy-duty truck in a 4-vehicle network. Numerical simulations are conducted to validate the analytical results and test the system performance.

3.1 Controller Design

For the high-level controller, we use the connected cruise control presented in [15]. That is,

$$\dot{x}_{\mathrm{ir}} = \begin{bmatrix} v_{\mathrm{ir}} \\ \sum_{j=i-n}^{i-1} \gamma_{i,j}\Big(\alpha_{i,j}\big(V(h_{\mathrm{ir},j}) - v_{\mathrm{ir}}\big) + \beta_{i,j}(v_j - v_{\mathrm{ir}})\Big) \end{bmatrix}, \tag{15}$$

cf. (4), where constants $\alpha_{i,j}, \beta_{i,j}$ are control gains corresponding to the average headway and relative velocity between vehicle i and vehicle j, respectively. The range policy function $V(h)$ gives the desired velocity according to the headway h. Here, we use

$$V(h) = \begin{cases} 0, & \text{if} \quad h \le h_{\mathrm{st}}, \\ \frac{v_{\max}}{2}\left[1 - \cos\left(\pi \frac{h - h_{\mathrm{st}}}{h_{\mathrm{go}} - h_{\mathrm{st}}}\right)\right], & \text{if} \quad h_{\mathrm{st}} < h < h_{\mathrm{go}}, \\ v_{\max}, & \text{if} \quad h \ge h_{\mathrm{go}}, \end{cases} \tag{16}$$

which indicates that the vehicle tends to stop for small distances $h \le h_{\mathrm{st}}$ and aims to keep the preset maximum velocity $v_{\max}$ for large distances $h \ge h_{\mathrm{go}}$. For $h_{\mathrm{st}} < h < h_{\mathrm{go}}$, the desired velocity is a monotonically increasing function of h. Note that the range policy function (16) is smooth at h_{st} and h_{go}, which can improve the drivers' comfort. According to traffic data [21], the parameter values are set as $h_{\mathrm{st}} = 5$ [m], $h_{\mathrm{go}} = 35$ [m], and $v_{\max} = 30$ [m/s].

Then, one needs to design control gains $\alpha_{i,j}$ and $\beta_{i,j}$ to guarantee asymptotic stability of the equilibrium (2). According to the range policy function (16), the domains of interest are

$$\mathscr{D}_h = \{h : h_{\mathrm{st}} < h < h_{\mathrm{go}}\}, \quad \mathscr{D}_v = \{v : 0 < v < v_{\max}\}. \tag{17}$$

Then, by applying Theorem 1 to system (15), we obtain the condition for choosing control gains $\alpha_{i,j}$ and $\beta_{i,j}$ as stated in the following theorem.

Theorem 3. *The equilibrium of the high-level controller* (15) *is asymptotically stable if, for a chosen constant $\mu > 0$, the control gains satisfy*

$$\begin{aligned} \sum_{j=i-n}^{i-1} \gamma_{i,j}(\alpha_{i,j} + \beta_{i,j}) &> \mu, \\ \sum_{j=i-n}^{i-1} \gamma_{i,j}\left(\Big(-\frac{\pi}{8(i-j)\mu} + 1\Big)\alpha_{i,j} + \beta_{i,j}\right) &> \mu. \end{aligned} \tag{18}$$

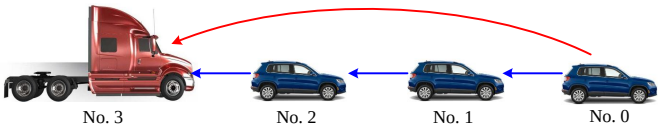

FIGURE 3. A vehicle network where the CCC vehicle 3 reacts to vehicle 0 and vehicle 2 while other vehicles only react to the vehicle immediately ahead. Blue links can be realized by human perception, range sensors, or V2V communication, while the red link can only be realized by using V2V communication.

The proof is given in Appendix C. Note that (18) is a sufficient condition for the asymptotic stability of the equilibrium. When using Theorem 3, one can begin by setting a positive value for μ. Then, the inequalities (18) determine the stable domain for the control gains. Specific stable domains were demonstrated in [22] for a simple network. We remark that choosing different values for μ will lead to different stability domains.

When designing the low-level controller, we refer to the framework (11)–(14) and the function L given by (46) with constraints (47) and (50). It follows that the adaptive control strategy on the axle torque is given by

$$T_{\mathrm{a},i} = \hat{\theta}_{i,1} \sum_{j=i-n}^{i-1} \gamma_{i,j}\big(\alpha_{i,j}\big(V(h_{i,j}) - v_i\big) + \beta_{i,j}(v_j - v_i)\big) + \hat{\theta}_{i,2}\sin\phi + \hat{\theta}_{i,3}\cos\phi + \hat{\theta}_{i,4}v_i^2 \tag{19}$$

with the adaptation law

$$\dot{\hat{\theta}}_i = \Gamma w \big[Pe_i\big]_2, \tag{20}$$

where P is given by (47) and (50).

3.2 Simulations

Here, we apply the CCC design (19,20) to a 4-vehicle network shown in Fig. 3, where the CCC-equipped heavy-duty vehicle monitors the motion of vehicle 0 via V2V communication. We suppose that vehicle 1 is not equipped with V2V devices so that vehicle 3 cannot obtain motion information from this vehicle. Such connectivity structure corresponds to $\gamma_{3,0} = \gamma_{3,2} = 1$ and $\gamma_{3,1} = 0$ in (19). The parameters of the heavy-duty vehicle are provided in Appendix D. We presume that vehicle 0 follows the EPA New York city drive cycle [23] as shown in Fig. 4(a). The gear shift map used for the heavy-duty vehicle is provided in Fig. 4(b), where the blue and the red curves represent upshift and downshift, respectively. The torque demand is assumed to be proportional to the pedal position. We also assume constant road grade $\phi_i \equiv 2^\circ$ and constant speed of headwind $v_{\mathrm{w},i} = 4$ [m/s]. For

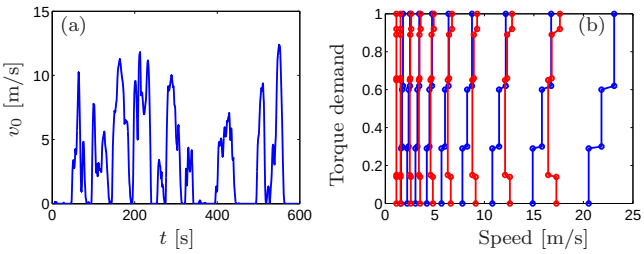

FIGURE 4. (a) Velocity profile of vehicle 0 that is generated by the EPA New York city drive cycle. (b) Gear shift map used for the heavy-duty vehicle, where blue and red curves indicate up and down shifts, respectively.

vehicles 1 and 2, we consider that they only react to the vehicle immediately ahead according to

$$\dot{x}_j = \begin{bmatrix} v_j \\ \alpha_{\mathrm{h}}\big(V(h_{j,j-1}) - v_i\big) + \beta_{\mathrm{h}}(v_{j-1} - v_j) \end{bmatrix}, \tag{21}$$

for $j = 1, 2$; cf. (15). Here, we use $\alpha_{\mathrm{h}} = 0.5$ [1/s] and $\beta_{\mathrm{h}} = 0.6$ [1/s].

According to (18) with $\mu = \pi/8$, the asymptotic stability of the equilibrium of the high-level controller can be guaranteed by the control gains $\alpha_{3,2} = 0.5$ [1/s], $\beta_{3,2} = 0.6$ [1/s], $\alpha_{3,0} = 0.2$ [1/s], and $\beta_{3,0} = 0.2$ [1/s]. And we use $p_2 = \pi$ and $p_3 = 8$ in (45,47,50) and obtain

$$P = \begin{bmatrix} (\alpha_{3,2} + \beta_{3,2} + \alpha_{3,0} + \beta_{3,0})\pi & \pi \\ \pi & 8 \end{bmatrix}, \tag{22}$$

which is used in the adaptation law of the low-level controller; cf. (20). Based on (10) and the values of parameters given in Appendix D, we have $\theta_3 \approx [8011,\ 78495,\ 471,\ 2]^{\mathrm{T}}$. But note that these vehicle parameters may not be available when designing controllers. For parameter adaptation, we set the initial condition as $\hat{\theta}_3 = [0,\ 0,\ 0,\ 0]^{\mathrm{T}}$. And we use the adaptation gain $\Gamma = \mathrm{diag}\{50,\ 4000,\ 50,\ 0.001\}$. Moreover, the initial states are set as follows: $[s_0(0),\ s_1(0),\ s_2(0),\ s_3(0)] = [0,\ -10,\ -25,\ -35]$ [m] and $v_i(0) = 0$ [m/s] for $i = 1, 2, 3$. We also assume identical vehicle length $l_k = 5$ [m] for $k = 0, 1, 2$ while the length of vehicle 3 is $l_3 = 20$ [m]. The simulation results are shown in Fig. 5, where panel (a) shows the state of vehicle 3 (black dashed-dotted curve) tracks the desired state (red solid curve). The axle torque required by the controller (11) is shown in Fig. 5(b). Fig. 5(c) and (d) show the corresponding engine torque and gears, respectively, which are obtained based on the gear shift map given in Fig. 4(b). The results indicate that the required engine torque is in the feasible range $T_{\mathrm{e}} \le T_{\mathrm{e,max}} = 2314.3$ [Nm]. Fig. 5(e)–(h) show that the adapted parameters do not converge to their real values,

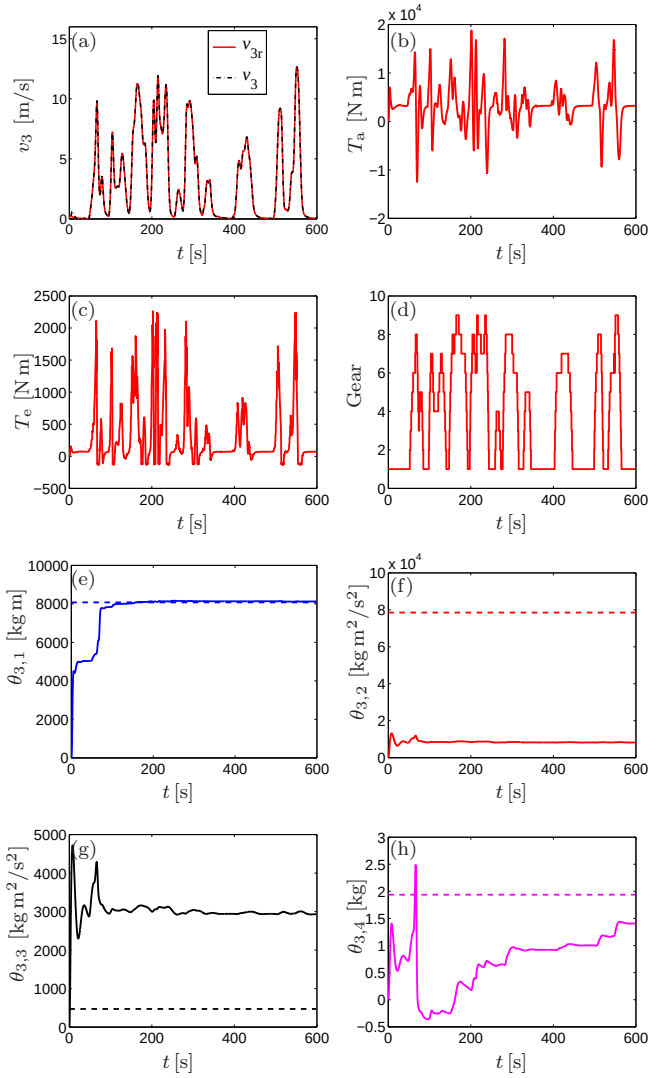

FIGURE 5. (a) Velocity of the CCC vehicle 3. The red solid curve denotes the reference state generated by the high-level controller while the black dashed-dotted curve denotes the vehicle's actual state. (b) Axle torque required by controller (19). (c) Corresponding engine torque. (d) Corresponding gear shifts. (e)–(h) Parameter adaptation (solid) and corresponding real parameter values (dashed).

but this does not jeopardize the state tracking performance of the system shown in Fig. 5(a).

To evaluate the performance of the presented adaptive controller, we also simulate the system using a non-adaptive controller. That is, the torque control strategy is given by (19) but with fixed values of $\hat{\theta}_i$. We consider the case with unknown parameters and guess the values as $\hat{m} = 29484$ [kg], $\hat{R} = 0.6$ [m], $\hat{k} = 7.6896$ [kg/m], and $\hat{r} = 0.09$ in (10), yielding $\hat{\theta}_3 \approx [17699, 173543, 1562, 5]^{\mathrm{T}}$. Then, we compare the desired states

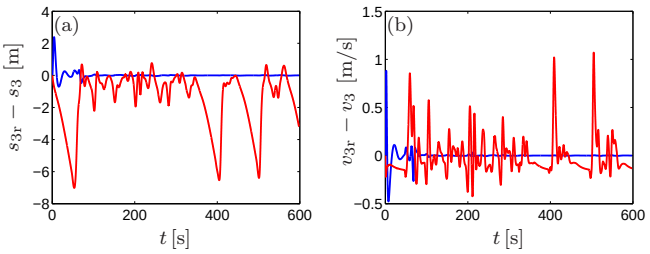

FIGURE 6. Difference between the desired states s_{3r}, v_{3r} and the vehicle states s_3, v_3 when using the adaptive low-level controller (blue) and using the non-adaptive controller (red), respectively.

s_{3r}, v_{3r} generated by the high-level controller with the states s_3, v_3, as shown in Fig. 6, where the blue curve is given by adaptive controller while the red curve is given by non-adaptive controller. It shows that the system with adaptive controller can track the desired motion while the system with non-adaptive controller produces significant errors. When the high-level controller is designed for minimizing fuel consumption or guaranteeing collision avoidance, large deviations from the desired states may increase fuel consumption or the collision risk. In this sense, the adaptive torque control leads to better performance than the non-adaptive control strategy.

4 CONCLUSIONS

In this paper, we presented a hierarchical framework to simplify the design of connected cruise control (CCC) that utilizes wireless vehicle-to-vehicle (V2V) communication. At the high level, a simplified vehicle model is used to design the connected car-following dynamics. At the low level, we use a physics-based vehicle model and design an adaptive controller, which enables the CCC vehicle to track the desired motion while compensating for external disturbances and uncertainties in physical parameters. After deriving stability conditions for the presented framework, we designed a specific CCC strategy. Numerical simulations for a 4-vehicle network validated the analytical results. In practice, V2V communication causes information delays due to the intermittency and packet drops, which may affect the system performance. In the future, we will extend this hierarchical framework for designing CCC in presence of communication delays. Moreover, the robustness of the presented adaptive controller against measurement noises and unmodeled dynamics will be also investigated.

REFERENCES

[1] van Arem, B., van Driel, C. J. G., and Visser, R., 2006. "The impact of cooperative adaptive cruise control on traffic-flow

characteristics". *IEEE Transactions on Intelligent Transportation Systems,* **7**(4), pp. 429–436.
[2] Alam, A., Gattamin, A., Johansson, K., and Tomlin, C., 2014. "Guaranteeing safety for heavy duty vehicle platooning: Safe set computations and experimental evaluations". *Control Engineering Practice,* **24**, pp. 33–41.
[3] Suthaputchakun, C., Sun, Z., and Dianati, M., 2012. "Applications of vehicular communications for reducing fuel consumption and CO_2 emission: the state of the art and research challenges". *IEEE Communications Magazine,* **50**(12), pp. 108–115.
[4] Zhao, Y., Minero, P., and Gupta, V., 2014. "On disturbance propagation in leader-follower systems with limited leader information". *Automatica,* **50**(2), pp. 591–598.
[5] Öncü, S., Ploeg, J., van de Wouw, N., and Nijmeijer, H., 2014. "Cooperative adaptive cruise control: network-aware analysis of string stability". *IEEE Transactions on Intelligent Transportation Systems,* **15**(4), pp. 1527–1537.
[6] Geiger, A., Lauer, M., Moosmann, F., Ranft, B., Rapp, H., Stiller, C., and Ziegler, J., 2012. "Team AnnieWAY's entry to the 2011 grand cooperative driving challenge". *IEEE Transactions on Intelligent Transportation Systems,* **13**(3), pp. 1008–1017.
[7] Robinson, T., Chan, E., and Coelingh, E., 2010. "Operating platoons on public motorways: an introduction to the SARTRE platooning programme". In Proceeings of the 17th World Congress on Intelligent Transport Systems.
[8] Milanés, V., and Shladover, S., 2014. "Modeling cooperative and autonomous adaptive cruise control dynamic responses using experimental data". *Transportation Research Part C,* **48**, pp. 285–300.
[9] Naus, G. J. L., Vugts, R. P. A., Ploeg, J., van de Molengraft, M. J. G., and Steinbuch, M., 2010. "String-stable CACC design and experimental validation: A frequency-domain approach". *IEEE Transactions on Vehicular Technology,* **59**(9), pp. 4268–4279.
[10] Zhang, L., and Orosz, G., 2013. "Designing network motifs in connected vehicle systems: delay effects and stability". In Proceedings of the ASME Dynamic Systems and Control Conference, p. V003T42A006.
[11] Ge, J. I., and Orosz, G., 2014. "Dynamics of connected vehicle systems with delayed acceleration feedback". *Transportation Research Part C,* **46**, pp. 46–64.
[12] Qin, W. B., Gomez, M. M., and Orosz, G., 2014. "Stability analysis of connected cruise control with stochastic delays". In American Control Conference, pp. 5534–5539.
[13] Seiler, P., Pant, A., and Hedrick, K., 2004. "Disturbance propagation in vehicle strings". *IEEE Transactions on Automatic Control,* **49**(10), pp. 1835–1842.
[14] Ploeg, J., Shukla, D. P., van de Wouw, N., and Nijmeijer, H., 2014. "Controller synthesis for string stability of vehicle platoons". *IEEE Transactions on Intelligent Transportation Systems,* **15**(2), pp. 854–865.
[15] Zhang, L., and Orosz, G., 2015. "Nonlinear connected vehicle system with communication delays". In American Control Conference, pp. 2759–2764.
[16] Alsabaan, M., Naik, K., and Khalifa, T., 2013. "Optimization of fuel cost and emissions using V2V communications". *IEEE Transactions on Intelligent Transportation Systems,* **14**(3), pp. 1449–1461.
[17] Althoff, M., Stursberg, O., and Buss, M., 2009. "Model-based probabilistic collision detection in autonomous driving". *IEEE Transactions on Intelligent Transportation Systems,* **10**(2), pp. 299–310.
[18] Ioannou, P., and Sun, J., 2012. *Robust adaptive control*. Courier Dover Publications.
[19] Ulsoy, A. G., Peng, H., and Çakmakci, M., 2012. *Automotive Control Systems*. Cambridge University Press.
[20] Orosz, G., 2014. "Connected cruise control: modeling, delay effects, and nonlinear behavior". *Vehicle System Dynamics*, p. submitted.
[21] Orosz, G., Wilson, R. E., and Stépán, G., 2010. "Traffic jams: dynamics and control". *Philosophical Transactions of the Royal Society A,* **368**(1928), pp. 4455–4479.
[22] Zhang, L., and Orosz, G., 2014. "Stability analysis of nonlinear connected vehicle systems". In Proceedings of the ASME Dynamic Systems and Control Conference, no. DSCC2014-6358, p. V001T10A006.
[23] US EPA dynamometer drive schedules. http://www.epa.gov/oms/emisslab/testing/dynamometer.htm.

A Proof of Theorem 1

At the equilibrium (2), the average headway between vehicle j and vehicle i (3) becomes

$$h^*_{\mathrm{ir},j} = \frac{s^*_j - s^*_{\mathrm{ir}} - \sum_{k=j}^{i-1} l_k}{i-j}. \tag{23}$$

To investigate the asymptotic stability of the equilibrium, we define the state perturbation of vehicle i as

$$\tilde{x}_{\mathrm{ir}} = \begin{bmatrix} \tilde{s}_{\mathrm{ir}} \\ \tilde{v}_{\mathrm{ir}} \end{bmatrix} = \begin{bmatrix} s_{\mathrm{ir}} - s^*_{\mathrm{ir}} \\ v_{\mathrm{ir}} - v^* \end{bmatrix}. \tag{24}$$

Substituting (1) and (2) into (4) and subtracting the result from (4) yields

$$\dot{\tilde{x}}_{\mathrm{ir}} = \begin{bmatrix} \tilde{v}_{\mathrm{ir}} \\ \sum_{j=i-n}^{i-1} \gamma_{i,j}\big(f_j(h_{\mathrm{ir},j}) + g_j(v_{\mathrm{ir}}) - f_j(h^*_{\mathrm{ir},j}) - g_j(v^*)\big) \end{bmatrix}. \tag{25}$$

When $h_{\mathrm{ir},j} \in \mathscr{D}_h$ and $v_{\mathrm{ir}} \in \mathscr{D}_v$ for $j = i-n, \ldots, i-1$, it follows that $h^*_{\mathrm{ir},j} \in \mathscr{D}_h$ and $v^*_{\mathrm{ir}} \in \mathscr{D}_v$. Then, based on the mean value theorem, there exist variables $\xi_j \in \mathscr{D}_h$ and $\varepsilon_j \in \mathscr{D}_v$ such that

$$\begin{aligned} f_j(h_{\mathrm{ir},j}) - f_j(h^*_{\mathrm{ir},j}) &= -\frac{f_j'(\xi_j)}{i-j}\tilde{s}_{\mathrm{ir}}\,, \\ g_j(v_{\mathrm{ir}}) - g_j(v^*) &= g_j'(\varepsilon_j)\tilde{v}_{\mathrm{ir}}\,. \end{aligned} \tag{26}$$

cf. (3), where $f_j'(h) = \mathrm{d}f_j/\mathrm{d}h$ and $g_j'(v) = \mathrm{d}g_j/\mathrm{d}v$. Indeed, the variables ξ_j and ε_j depend on states $h_{\mathrm{ir},j}$ and v_{ir}, respectively.

Substituting (26) into (25) yields

$$\dot{\tilde{x}}_{\mathrm{ir}} = A(\Psi)\tilde{x}_{\mathrm{ir}}\,, \tag{27}$$

where $\Psi = [\xi_{i-n}, \ldots, \xi_{i-1}, \varepsilon_{i-n}, \ldots, \varepsilon_{i-1}]^{\mathrm{T}} \in \mathscr{D}_h^n \times \mathscr{D}_v^n$ and

$$A(\Psi) = \begin{bmatrix} 0 & 1 \\ -\sum_{j=i-n}^{i-1} \frac{\gamma_{i,j}}{i-j} f_j'(\xi_j) & \sum_{j=i-n}^{i-1} \gamma_{i,j} g_j'(\varepsilon_j) \end{bmatrix}. \tag{28}$$

Thus, if there exists a Lyapunov function $L(\tilde{x}_{\mathrm{ir}}) \succ 0$ such that

$$\dot{L}(\tilde{x}_{\mathrm{ir}}) = \left[\frac{\partial L(\tilde{x}_{\mathrm{ir}})}{\partial \tilde{x}_{\mathrm{ir}}}\right]^{\mathrm{T}} A(\Psi)\tilde{x}_{\mathrm{ir}} \prec 0 \tag{29}$$

for $\forall \Psi \in \mathscr{D}_h^n \times \mathscr{D}_v^n$, it follows that $\tilde{x}_{\mathrm{ir}}(t) \to 0$ as $t \to \infty$ when $\tilde{x}_{\mathrm{ir}}(0)$ is sufficiently close to 0.

Based on (4), we have

$$\begin{aligned} &\frac{\partial F(x_{\mathrm{ir}}, x^*_{i-1}, \ldots, x^*_{i-n})}{\partial x_{\mathrm{ir}}} \\ &= \begin{bmatrix} 0 & 1 \\ -\sum_{j=i-n}^{i-1} \frac{\gamma_{i,j}}{i-j} f_j'(h_{\mathrm{ir},j}) & \sum_{j=i-n}^{i-1} \gamma_{i,j} g_j'(v_{\mathrm{ir}}) \end{bmatrix}. \end{aligned} \tag{30}$$

Comparing (28) with (30) shows that $A(\Psi)$ is equivalent to $\frac{\partial F(x_{\mathrm{ir}}, x^*_{i-1}, \ldots, x^*_{i-n})}{\partial x_{\mathrm{ir}}}$ in terms of bound as $\xi_j, h_{\mathrm{ir},j} \in \mathscr{D}_h$ and $\varepsilon_j, v_{\mathrm{ir}} \in \mathscr{D}_v$. Thus, (29) is equivalent to (6), which proves the theorem.

B Proof of Theorem 2

Substituting (11,12) into (9) leads to

$$\begin{aligned} \theta_{i,1}\dot{v}_i = \hat{\theta}_{i,1} &\sum_{j=i-n}^{i-1} \gamma_{i,j}\big(f_j(h_{i,j}) + d_j(v_j) + g_j(v_i)\big) \\ &- \tilde{\theta}_{i,2}\sin\phi_i - \tilde{\theta}_{i,3}\cos\phi_i - \tilde{\theta}_{i,4}(v_i + v_{\mathrm{w}})^2\,, \end{aligned} \tag{31}$$

where $\tilde{\theta}_{i,k} = \theta_{i,k} - \hat{\theta}_{i,k}$ $(k = 1,2,3,4)$ denote the difference between the real value of the parameters and those used in the adaptive controller. Dividing both sides by $\theta_{i,1}$, subtracting the result from the second equation of (4), and considering (13), we obtain

$$\begin{aligned} \dot{e}_{i,s} &= e_{i,v}\,, \\ \dot{e}_{i,v} &= \sum_{j=i-n}^{i-1} \gamma_{i,j}\big(f_j(h_{\mathrm{ir},j}) - f_j(h_{i,j}) + g_j(v_{\mathrm{ir}}) - g_j(v_i)\big) + \theta_{i,1}^{-1} w^{\mathrm{T}}\tilde{\theta}_i\,, \end{aligned} \tag{32}$$

where w is given by (12).

We assume that $h_{i,j}, v_i$ have the same bounds with $h_{\mathrm{ir},j}, v_{\mathrm{ir}}$, respectively. That is, $h_{i,j}, h_{\mathrm{ir},j} \in \mathscr{D}_h$ and $v_i, v_{\mathrm{ir}} \in \mathscr{D}_v$. Hence, according to the mean value theorem, there exist variables $\zeta_j \in \mathscr{D}_h$ and $\delta_j \in \mathscr{D}_v$ such that

$$\begin{aligned} f_j(h_{\mathrm{ir},j}) - f_j(h_{i,j}) &= -\frac{f_j'(\zeta_j)}{i-j} e_{i,s}\,, \\ g_j(v_{\mathrm{ir}}) - g_j(v_i) &= g_j'(\delta_j) e_{i,v}\,. \end{aligned} \tag{33}$$

Substituting (33) into (32), we obtain

$$\begin{aligned} \dot{e}_{i,s} &= e_{i,v}\,, \\ \dot{e}_{i,v} &= \sum_{j=i-n}^{i-1} \gamma_{i,j}\left(-\frac{f_j'(\zeta_j)}{i-j} e_{i,s} + g_j'(\delta_j) e_{i,v}\right) + \theta_{i,1}^{-1} w^{\mathrm{T}}\tilde{\theta}_i\,. \end{aligned} \tag{34}$$

Writing (34) in the matrix form yields

$$\dot{e}_i = A(\Omega) e_i + \theta_{i,1}^{-1} w_{\mathrm{aug}}^{\mathrm{T}}\tilde{\theta}_i\,, \tag{35}$$

where $\Omega = [\zeta_{i-n}, \ldots, \zeta_{i-1}, \delta_{i-n}, \ldots, \delta_{i-1}] \in \mathscr{D}_h^n \times \mathscr{D}_v^n$, $A(\Omega)$ is given by (28) when substituting $\xi_j = \zeta_j$ and $\varepsilon_j = \delta_j$, and

$$w_{\mathrm{aug}} = [\mathbf{0}_{4\times 1}\,,\ w] \in \mathbb{R}^{4\times 2}\,, \tag{36}$$

where $\mathbf{0}_{4\times 1}$ is a 4-by-1 zero vector.

Then, we prove the asymptotic stability of $e_i = 0$ by using the Lyapunov function

$$V(e_i, \tilde{\theta}_i) = L(e_i) + \frac{1}{2}\theta_{i,1}^{-1}\tilde{\theta}_i^{\mathrm{T}}\Gamma^{-1}\tilde{\theta}_i\,, \tag{37}$$

where $L(e_i) \succ 0$ is the Lyapunov function used in Theorem 1 if x_{ir} is replaced by e_i, and $\Gamma \succ 0$ is a constant matrix. From (10), we have $\theta_{i,1} > 0$ and thus $V(e_i, \tilde{\theta}_i) \succ 0$.

Differentiating (37) with respect to time and substituting (35) into the result leads to

$$\dot{V}(e_i,\tilde{\theta}_i)=\left[\frac{\partial L(e_i)}{\partial e_i}\right]^{\mathrm{T}}A(\Omega)e_i+\theta_{i,1}^{-1}\tilde{\theta}_i^{\mathrm{T}}\left(w_{\mathrm{aug}}\frac{\partial L(e_i)}{\partial e_i}-\Gamma^{-1}\dot{\hat{\theta}}_i\right). \tag{38}$$

According to (36), the first column of the vector w_{aug} only consists of zeros, resulting in

$$w_{\mathrm{aug}}\frac{\partial L(e_i)}{\partial e_i}=w\left[\frac{\partial L(e_i)}{\partial e_i}\right]_2. \tag{39}$$

Substituting (14) and (39) into (38) yields

$$\dot{V}(e_i,\tilde{\theta}_i)=\left[\frac{\partial L(e_i)}{\partial e_i}\right]^{\mathrm{T}}A(\Omega)e_i. \tag{40}$$

If Theorem 1 holds, we have $\dot{V}(e_i,\tilde{\theta}_i)\preceq 0$ for $\forall\Omega\in\mathscr{D}_h^n\times\mathscr{D}_v^n$. The largest invariant set in $\dot{V}(e_i,\tilde{\theta}_i)=0$ is $e_i=0$, implying that $e_i(t)\to 0$ as $t\to\infty$ when $e_i(0)$ is chosen sufficiently close to 0. Note that since $\dot{V}(e_i,\tilde{\theta}_i)$ is independent of $\tilde{\theta}_i$, Theorem 2 does not guarantee $\tilde{\theta}_i(t)\to 0$ as $t\to\infty$.

C Proof of Theorem 3

Let vehicles $j=i-1,\dots,i-n$ move at the equilibrium, i.e., $x_j(t)=x_j^*(t)$. Substituting $x_{i\mathrm{r}}(t)=x_{i\mathrm{r}}^*(t)$ into (15) and subtracting the result from (15) yields

$$\dot{\tilde{x}}_{i\mathrm{r}}=\begin{bmatrix}\tilde{v}_{i\mathrm{r}}\\ \sum_{j=i-n}^{i-1}\alpha_{i,j}\big(V(h_{i\mathrm{r},j})-V(h_{i\mathrm{r},j}^*)\big)-(\alpha_{i,j}+\beta_{i,j})\tilde{v}_{i\mathrm{r}}\end{bmatrix}, \tag{41}$$

where $\tilde{x}_{i\mathrm{r}}$ is defined in (24). Compared with (25), we have

$$f_j(h_{i\mathrm{r},j})=\alpha_{i,j}V(h_{i\mathrm{r},j}),\quad g_j(v_{i\mathrm{r}})=-(\alpha_{i,j}+\beta_{i,j})v_{i\mathrm{r}}. \tag{42}$$

Considering $h_{i\mathrm{r},j},h_{i\mathrm{r},j}^*\in\mathscr{D}_h$ and $v_{i\mathrm{r}},v_{i\mathrm{r}}^*\in\mathscr{D}_v$ and using the mean value theorem, there exist variables $\xi_j\in\mathscr{D}_h$ and $\varepsilon_j\in\mathscr{D}_v$ such that

$$\begin{aligned}f(h_{i\mathrm{r},j})-f(h_{i\mathrm{r},j}^*)&=-\frac{f'(\xi_j)}{i-j}\tilde{s}_{i\mathrm{r}}=-\frac{\alpha_{i,j}V'(\xi_j)}{i-j}\tilde{s}_{i\mathrm{r}},\\ g(v_{i\mathrm{r}})-g(v_{i\mathrm{r}}^*)&=g'(\varepsilon_j)\tilde{v}_{i\mathrm{r}}=-(\alpha_{i,j}+\beta_{i,j})\tilde{v}_{i\mathrm{r}},\end{aligned} \tag{43}$$

cf. (26). Substituting (43) into (41) yields (27), where $\Psi=[\xi_{i-n},\ \dots,\ \xi_{i-1},\ \varepsilon_{i-n},\ \dots,\ \varepsilon_{i-1}]\in\mathscr{D}_h^n\times\mathscr{D}_v^n$ and

$$A(\Psi)=\begin{bmatrix}0 & 1\\ -\varphi(\Psi) & -\kappa\end{bmatrix}, \tag{44}$$

with

$$\varphi(\Psi)=\sum_{j=i-n}^{i-1}\frac{\gamma_{i,j}\alpha_{i,j}}{i-j}V'(\xi_j),\quad \kappa=\sum_{j=i-n}^{i-1}\gamma_{i,j}(\alpha_{i,j}+\beta_{i,j}). \tag{45}$$

cf. (28). If there exists a Lyapunov function

$$L=\tilde{x}_{i\mathrm{r}}^{\mathrm{T}}P\tilde{x}_{i\mathrm{r}}\succ 0,\quad \dot{L}=\tilde{x}_{i\mathrm{r}}^{\mathrm{T}}\big(A^{\mathrm{T}}(\Psi)P+PA(\Psi)\big)\tilde{x}_{i\mathrm{r}}\prec 0, \tag{46}$$

then the equilibrium $\tilde{x}_{i\mathrm{r}}(t)=0$ is asymptotically stable. To satisfy (46), the matrix P must be positive definite, yielding

$$P=\begin{bmatrix}p_1 & p_2\\ p_2 & p_3\end{bmatrix},\quad p_1>0,\quad p_3>0,\quad p_1p_3-p_2^2>0. \tag{47}$$

To guarantee $\dot{L}\prec 0$ in (46), it requires that $A^{\mathrm{T}}(\Psi)P+PA(\Psi)\prec 0$ for $\forall\Psi\in\mathscr{D}_h^n\times\mathscr{D}_v^n$, which is equivalent to that the coefficients of the characteristic polynomial

$$\det\big(\lambda I_2-A^{\mathrm{T}}(\Psi)P-PA(\Psi)\big)=\lambda^2+\rho_1\lambda+\rho_0 \tag{48}$$

are positive for $\forall\Psi\in\mathscr{D}_h^n\times\mathscr{D}_v^n$, that is,

$$\begin{aligned}&\rho_1=2(\varphi-1)p_2+2\kappa p_3>0,\\ &\rho_0=-p_3^2\varphi^2+2(p_1p_3-2p_2^2+\kappa p_2p_3)\varphi-(p_1-\kappa p_2)^2>0.\end{aligned} \tag{49}$$

For $\rho_0>0$, we need

$$p_1-\kappa p_2=0, \tag{50}$$

which implies $p_2=p_1/\kappa>0$. Substituting (45) and (50) into (49) leads to

$$\begin{aligned}&\sum_{j=i-n}^{i-1}\gamma_{i,j}\big(\big(p_3+V'(\xi_j)p_2\big)\alpha_{i,j}+p_3\beta_{i,j}\big)>p_2,\\ &\sum_{j=i-n}^{i-1}\gamma_{i,j}\bigg(\Big(-\frac{p_3^2}{i-j}V'(\xi_j)+4p_2p_3\Big)\alpha_{i,j}+4p_2p_3\beta_{i,j}\bigg)>4p_2^2.\end{aligned} \tag{51}$$

To ensure the inequalities in (51), the minimum of the left hand sides must be positive in the domain (17), which corresponds to $0\le V'(\xi_j)\le\pi/2$; cf. (16). For positive control gains $\alpha_{i,j},\beta_{i,j}>0$, this leads to the condition (18) with $\mu=p_2/p_3$. Choosing the matrix P according to (47) and (50) while designing control gains satisfying (18), the Lyapunov stability condition (46) holds so that $\tilde{x}_{i\mathrm{r}}(t)\to 0$ as $t\to\infty$ if the $\tilde{x}_{i\mathrm{r}}(0)$ is chosen sufficiently close to 0.

D Physical Vehicle Parameters

Parameter	Value
Mass (m)	15876 [kg]
Air Drag Coefficient (k)	3.8448 [kg/m]
Tire Rolling Radius (R)	0.5040 [m]
Tire Rolling Resistance Coefficient (r)	0.006
Engine Rotational Inertia (J)	5 [$\mathrm{kg\,m^2}$]
Gravitational Constant (g)	9.81 [$\mathrm{m/s^2}$]
Maximum Engine Torque	2314.3 [$\mathrm{N\,m}$]
Number of Forward Gears	10
1st Gear Ratio	12.94
2nd Gear Ratio	9.29
3rd Gear Ratio	6.75
4th Gear Ratio	4.90
5th Gear Ratio	3.62
6th Gear Ratio	2.64
7th Gear Ratio	1.90
8th Gear Ratio	1.38
9th Gear Ratio	1.00
10th Gear Ratio	0.74
Final Drive Ratio	3.73